13th International Conference on Applications of Statistics and Probability in Civil Engineering, ICASP13
Seoul, South Korea, May 26-30, 2019

Hazard-Consistent Intensity Measure Conversion of Fragility Curves

Akiko Suzuki
Graduate Student, Dipartimento di Strutture per l'Ingegneria e l'Architettura, Università degli Studi di Napoli Federico II, Naples, Italy

Iunio Iervolino
Professor, Dipartimento di Strutture per l'Ingegneria e l'Architettura, Università degli Studi di Napoli Federico II, Naples, Italy

ABSTRACT: In seismic risk assessment of structures, fragility functions are the typical representation of seismic vulnerability, expressing the probability of exceedance of a given performance level as a function of a ground motion intensity measure (IM). Fragility curves, in general, are structure- and site-specific, thus a comparison of fragility curves is not straightforward across multiple structures and/or sites. The study presented in this paper discusses possible strategies to convert a fragility curve from an original IM to a target IM for a given site. In particular, three conversion cases, under different assumptions on the explanatory power with respect to structural failure of the involved IMs, are considered: (i) a vector-valued IM consisting of two different IMs (to say, original and target), magnitude, and source-to-site distance, (ii) a vector-valued IM consisting of the original and target IMs, and (iii) the original IM only, supposed to be a *sufficient* one; i.e., the structural response given IM statistically-independent of the other ground motion characteristics. The original fragility functions are supposed to be obtained through the state-of-the-art methods, then the fragility functions in terms of the target IM are obtained via applications of the probability calculus rules, which ensure consistency with the seismic hazard at the site of interest. The considered cases are illustrated via an example referring to an Italian code-conforming RC building designed for a site in L'Aquila. As far as the case-study is concerned, all conversion cases show agreement, likely because of the hazard-consistent record selection and to the explanatory power of the original IM with respect to structural failure.

1. INTRODUCTION

Probabilistic seismic risk assessment of structures evaluates the mean annual frequency of exceeding a given performance level (i.e., *failure rate*) by integrating seismic fragility and seismic hazard, both expressed in terms of the same ground motion (GM) intensity measure (IM) serving as a link between the two probabilistic models. The choice of the IM to be employed in the risk analysis is structure-specific. In principle, it is mainly determined by the desired properties of the selected IM, e.g., *sufficiency* and *efficiency*, and also considering issues such as *robustness* to GM scaling (Tothong and Luco, 2007).

In earthquake engineering practice, the peak ground acceleration (PGA) and the spectral acceleration at the fundamental vibration period of the structure, $Sa(T)$, are common IMs. PGA is convenient because hazard models are typically developed in terms of PGA. $Sa(T)$ is generally considered more efficient than PGA, and sufficient in several situations. Hence, it is often used as the IM for the development of fragility functions; however, fragility expressed in terms of spectral acceleration at different vibration periods cannot be directly compared.

Several studies addressed approaches for converting IMs of fragility curves in the last decades. For example, Ohtori and Hirata (2007)

presented an approach based on the *first-order second moment* approximation although the relationship between original and target IMs (to convert from and to, denoted as IM_1 and IM_2, respectively) is not completely characterized. Michel et al. (2018) recently proposed a probabilistic approach to convert fragility curves to a common IM considering the conditional probability of IM_2 given IM_1, yet the converted fragility functions in terms of IM_2 are conditional to a specific earthquake scenario, beyond IM_2. Furthermore, these past studies seem to assume IM_1 of a specific structure to be sufficient, which is not the general case.

Aiming at discussing fragility conversion between spectral accelerations in a rigorous probabilistic framework, the study presented herein examines three conversion cases, with different assumptions on the IMs involved. In particular, the fragility curve of a structure in terms of the target intensity (i.e., IM_2) is derived through hazard-consistent conversion of a fragility function varying the number of the original IMs; i.e., IM_1, IM_2 and the GM characteristics for hazard assessment of the site. The IMs considered in each case are: (i) a vector-valued intensity measure ($\mathbf{IM}$) consisting of IM_1, IM_2, magnitude (M) and source-to-site distance (R), hereafter denoted as $\mathbf{IM}_{4\mathrm{v}}$; (ii) a vector-valued $\mathbf{IM}$ consisting of IM_1 and IM_2, hereafter denoted as $\mathbf{IM}_{2\mathrm{v}}$; and (iii) the original IM_1 which is supposed to be a sufficient IM.

The converted fragility functions are obtained with the state-of-the-art methods for structural response analysis within the *Performance-Based Earthquake Engineering* framework (PBEE; Cornell and Krawinkler, 2000), which ensures consistency with the earthquake scenarios at the site of interest; i.e., the *multiple stripe analysis* method (MSA; Jalayer and Cornell, 2003), and hazard-consistent record selection based on the *conditional spectra* (CS; Lin et al., 2013).

The considered cases are investigated for an Italian code-conforming RC building for which the fragility conversion is performed from the spectral acceleration at a period close to the fundamental vibration period of the structure (i.e., IM_1) to PGA (i.e., IM_2). For comparison, a fragility curve expressed in terms of IM_2 (i.e., PGA) is also evaluated by performing nonlinear dynamic analyses (NLDAs) carried out with reference to IM_2.

2. METHODOLOGY

The considered framework assumes that structural response data are obtained through NLDA, aiming to assess the fragility in terms of IM_1, and intends to convert to IM_2 without carrying out further structural analyses.

2.1. Conversion equations

When *structural failure* (denoted as *F*) is defined as the exceedance of a given performance level, the probability of failure given a certain (y) value of the target IM_2, that is $P\left[F \mid IM_2 = y\right]$, can be computed via Eq. (1) based on the total probability theorem. In the equation: the first term of the integrands $P\left[F \middle| IM_1 = x \cap IM_2 = y \cap M = w \cap R = z\right]$ is the failure probability conditional to $\{IM_1, IM_2, M, R\}$; $f_{IM_1,M,R|IM_2}(x,w,z \mid y)$ is a probability density function (PDF), given by the product of the following two PDFs: $f_{IM_1|IM_2,M,R}\left(x \middle| y,w,z\right)$ and $f_{M,R|IM_2}\left(w,z \middle| y\right)$. The former can be obtained from a ground motion prediction equation (GMPE), considering the statistical dependency between IM_1 and IM_2 conditional to M and R, while the latter is computed through seismic hazard *disaggregation* (e.g., Bazzurro and Cornell, 1999) that provides the probability (density) of a certain M and R scenario given the occurrence of IM_2.

$$P\left[F \middle| IM_2 = y\right] = \int_{IM_1}\int_{M}\int_{R} P\left[F \middle| IM_1 = x \cap IM_2 = y \cap M = w \cap R = z\right] \cdot f_{IM_1,M,R|IM_2}(x,w,z \mid y) \cdot dz \cdot dw \cdot dx \quad (1)$$

If the vector $\{IM_1, IM_2\}$ is a sufficient **IM**, the structural response given **IM** is, by definition, statistically-independent of M and R, and Eq. (1) can be reduced to Eq. (2).

If the original IM_1 is a sufficient one (also with respect to IM_2), then Eq. (2) can be further simplified as per Eq. (3).

2.2. Fragility modelling

The fragility functions within the integrals at the right-hand sides of Eqs. (1)-(3) can be obtained via NLDA, which provides the seismic demand in terms of an Engineering Demand Parameter (EDP). The modelling approaches discussed herein assume structural assessment procedures such as the *cloud method* (Cornell et al., 2002) and MSA method. The former typically employs a set of unscaled GM records, while the latter approach employs, for different values of IM_1, different record sets each of which is selected consistent with the seismic hazard at the site of interest in terms of IM_1.

Log-linear regression models are often employed to calibrate the relationship between the EDP and IMs. For example, in the case of $\mathbf{IM}_{4v}$, the logarithm of EDP, in its simplest format, is given by Eq. (4), where $\ln \overline{EDP}$ is the conditional mean, $\{\beta_0, \beta_1, \beta_2, \beta_3, \beta_4\}$ are regression coefficients, and η (i.e., the regression residual) is a zero-mean Gaussian random variable, with standard deviation σ_η. At this point, if EDP_f is a threshold identifying failure, the lognormal fragility is given by Eq. (5) (Baker, 2007).

It should be noted that the numerical model of the structure does not yield meaningful EDP values in cases *numerical instability*, according to the definition in Shome and Cornell (2000), occurs. Even in such cases, one can derive a fragility model that accounts for the contribution from these data (e.g., Elefante et al., 2010).

Furthermore, in case of MSA, the fragility function can be also modelled estimating different regression coefficients for each IM_1 stripe (an option not considered in the following application).

2.3. Hazard terms

The calculations to obtain $f_{IM_1|IM_2,M,R}$ have been discussed in previous research (e.g., Baker and Cornell, 2005; Iervolino et al., 2010) Provided that T_1 and T_2 denote the vibration periods corresponding to $IM_1 = Sa(T_1)$ and $IM_2 = Sa(T_2)$, it is often assumed that $f_{IM_1|IM_2,M,R}$ is a lognormal distribution. The mean value of $\ln IM_1$ given $\{\ln IM_2, M, R\}$ and the standard deviation of $\ln IM_1$ given $\ln IM_2$, denoted as $\mu_{\ln IM_1|\ln IM_2,M,R}$ and $\sigma_{\ln IM_1|\ln IM_2}$, respectively, can be calculated as:

$$\begin{cases} \mu_{\ln IM_1|\ln IM_2,M,R} = \mu_{\ln IM_1|M,R} + \rho_{T_1,T_2} \cdot \varepsilon_{T_2} \cdot \sigma_{\ln IM_1} \\ \sigma_{\ln IM_1|\ln IM_2} = \sqrt{1-\rho_{T_1,T_2}^2} \cdot \sigma_{\ln IM_1} \end{cases} \quad (6)$$

where $\mu_{\ln IM_1|M,R}$ and $\sigma_{\ln IM_1}$ are the mean and standard deviation of $\ln IM_1$ conditional to M and R (i.e., from a GMPE), ρ_{T_1,T_2} is the correlation coefficient between the logarithms of

$$P\left[F \middle| IM_2 = y\right] = \int_{IM_1}\int_M\int_R P\left[F \middle| IM_1 = x \cap IM_2 = y\right] \cdot f_{IM_1,M,R|IM_2}(x,w,z \mid y) \cdot dz \cdot dw \cdot dx \quad (2)$$

$$P\left[F \middle| IM_2 = y\right] = \int_{IM_1}\int_M\int_R P\left[F \middle| IM_1 = x\right] \cdot f_{IM_1,M,R|IM_2}(x,w,z \mid y) \cdot dz \cdot dw \cdot dx \quad (3)$$

$$\ln EDP = \ln \overline{EDP} + \eta = \beta_0 + \beta_1 \cdot \ln x + \beta_2 \cdot \ln y + \beta_3 \cdot w + \beta_4 \cdot \ln z + \eta \quad (4)$$

$$P\left[F \middle| \mathbf{IM}\right] = P\left[EDP > EDP_f \middle| \mathbf{IM}\right] = 1 - \Phi\left(\frac{\ln EDP_f - \ln \overline{EDP}}{\sigma_\eta}\right) \quad (5)$$

the two IMs, and ε_{T_2} is the number of the standard deviations by which $\ln IM_2$ is away from the mean conditional to M and R (provided by the GMPE). Finally, $f_{M,R|IM_2}$ can be computed via hazard disaggregation.

3. ILLUSTRATIVE EXAMPLE

3.1. Structure and site

This study considered, as an example, one of the code-conforming RC residential buildings examined in the RINTC project; see Ricci et al. (2018) for details. In particular, the selected case study is the equivalent single-degree-of-freedom (ESDoF) system of the six-story 5×3 bay RC *pilotis*-frame building in Figure 1a. The building is supposed to be located in L'Aquila, central Italy (42.35° N, 13.40° E, on soil C-type, according to Eurocode 8 classification; see CEN, 2004). The ESDoF system was calibrated according to Baltzopoulos et al. (2017); i.e., leading to the ESDoF mass m^*, vibration period T^*, the critical viscous damping ratio ξ^*, and the characterizations of the hysteretic behavior for the static pushover (SPO) backbone. Figure 1b shows the tri-linear backbones of the ESDoF systems for the two horizontal directions (X and Y in Figure 1a). Each backbone of the ESDoF system is compared with that of the original three dimensional (3D) structural model scaled by the modal participation factor of the first-mode vibration, Γ. In the figure, the definitions of backbone parameters, that is, yield strength and displacement $\left(F_y^*, \delta_y^*\right)$, post-yielding hardening and softening ratio $\left(a_h, a_c\right)$, capping ductility $\left(\mu_c = \delta_c^* / \delta_y^*\right)$, and the residual strength ratio $\left(r_p\right)$, are also illustrated.

The EDP was defined as the demand-capacity (D/C) ratio of the roof-top displacement (i.e., $EDP_f = 1$) and the end of each backbone corresponds to the failure ductility $\left(\mu_f = \delta_f^* / \delta_y^*\right)$, which was defined on the basis of the displacement that determines a 50% drop from the maximum base-shear on the original structure's SPO curve. These parameters, including the yielding spectral acceleration at the equivalent vibration period $Sa_y\left(T^*\right)$, are summarized in Table 1 and Table 2.

Finally, a moderately-pinching, peak-oriented hysteretic behavior without any cyclic stiffness/strength deterioration (e.g., Vamvatsikos and Cornell, 2006), was applied to the ESDoF system. For more detailed information on structural features, see Suzuki et al. (2018).

3.2. Original fragilities

To derive the original fragilities, MSA was performed for ten IM, that is $Sa\left(T = 0.5s\right)$, values (i.e., *stripes*). The considered values correspond to exceedance return periods $\left(T_R\right)$ ranging from 10 to 10^5 at the site, in line with the framework of the aforementioned RINTC project. For each stripe, 20 GM records were collected based on the CS method (Iervolino et al., 2018) then the EDP was measured for each record. Figure 2 shows the mean spectra of the GM records and the obtained D/C ratios for all stripes

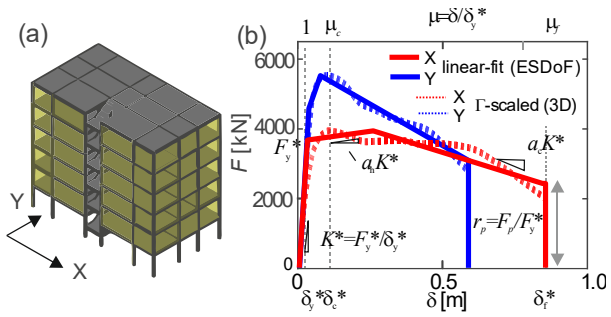

Figure 1: Case study RC building;
(a) 3D model; (b) SPO curves.

Table 1: Dynamic parameters of the ESDoF system.

Dir.	T^*	m^*	Γ	$Sa_y\left(T^*\right)$	ξ^*
X	0.65	1401	1.26	0.27	5%
Y	0.57	1251	1.33	0.37	5%

Table 2: SPO parameters of the ESDoF system.

Dir.	F_y^*	δ_y^*	a_h	μ_c	a_c	r_p	μ_f
X	3671	0.03	0.01	9.0	-0.02	0.66	30.0
Y	4581	0.03	0.17	2.2	-0.03	0.67	17.9

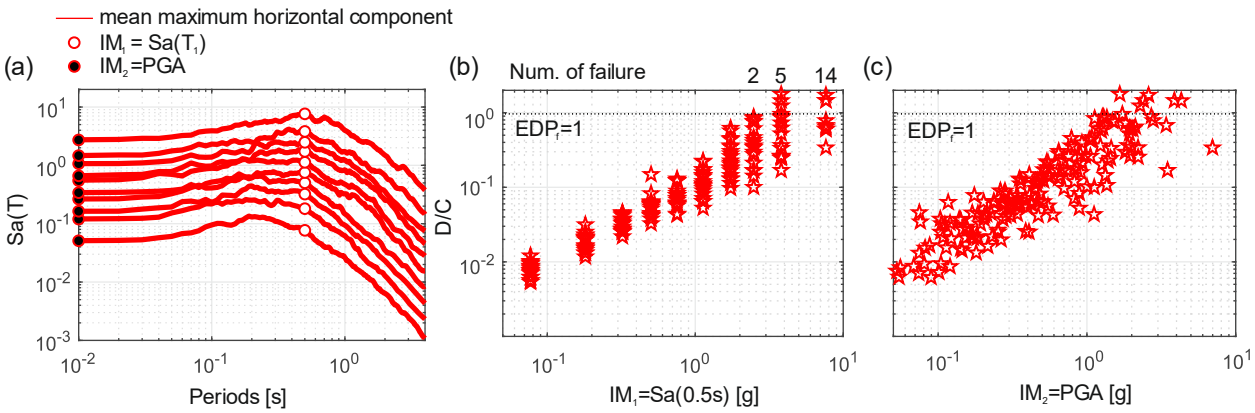

Figure 2: MSA for original fragility; (a) mean spectra of GM records; (b),(c) D/C ratios for the two IMs.

of IM_1, against the two IMs. The observed trends are then characterized by performing regression analysis via Eq. (4).

Given the response data from NLDA, the multiple linear regression analyses were performed with Eq. (4) varying the number of the intensity measures involved in the computation. According to the adopted GMPE (to follow), the considered Sa -based IM is the maximum horizontal acceleration response, and the considered GM characteristics were surface wave magnitude and *Joyner-Boore distance* (R_{jb} ; Joyner and Boore, 1981). Table 3 provides the regression results corresponding to the three IM cases. It is observed that the joint consideration of all four variables resulted in the lowest σ_η . Nonetheless, all the cases showed a comparable standard deviation of the residuals.

Table 3: Multiple linear regression analysis results.

IM	β_0	β_1	β_2	β_3	β_4	σ_η
$\mathbf{IM}_{4v}$	-2.71	0.72	0.19	0.14	-0.11	0.41
$\mathbf{IM}_{2v}$	-2.12	0.88	0.17	-	-	0.43
IM_1	-2.23	1.03	-	-	-	0.44

For each case, the related fragility function (i.e., $P\left[F\left|\mathbf{IM}\right.\right]$) was derived using Eqs. (4)-(5). As an example, the computed fragility (surface) is shown in Figure 3 for the case of $\mathbf{IM}_{2v}$. It can be seen that the failure probability increases principally with IM_1 and mildly with IM_2 for a given IM_1, which reflects the regression results in Table 3.

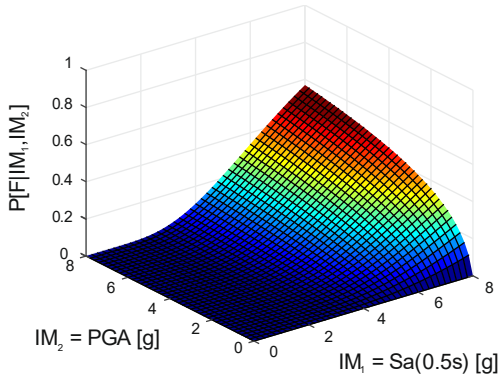

Figure 3: Fragility surface for the $\mathbf{IM}_{2v}$ *case.*

3.3. Hazard

PSHA was performed to characterize the conditional distribution $f_{IM_1|IM_2,M,R}$ for the site of interest. For the conditional PDF of IM_1 given IM_2 , this study employed the GMPE by Ambraseys et al. (1996) with the correlation coefficients proposed by Baker and Jayaram (2008). The correlation coefficient between PGA and $Sa(0.5s)$ was $\rho_{T_1,T_2} = 0.68$.

To perform hazard disaggregation for the site, this study utilized REASSESS (Chioccarelli et al., 2018) considering the Branch 921 of the official Italian hazard model (Stucchi et al., 2011) and the GMPE cited above.

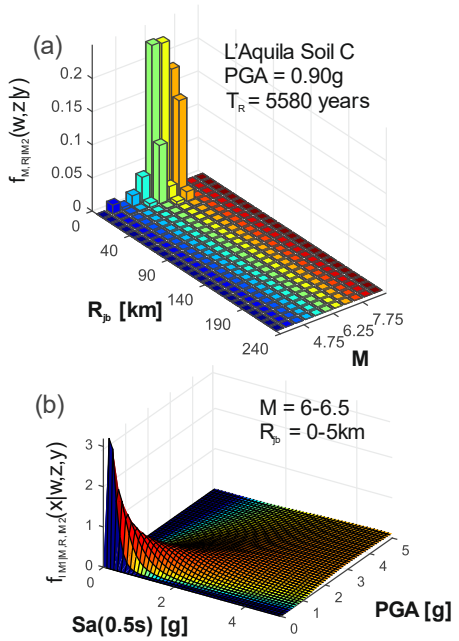

Figure 4: PSHA results;(a) hazard disaggregation for PGA = 0.90g corresponding to $T_R = 5580$ yrs at L'Aquila; (b) example of conditional PDF of $Sa(0.5s)$ given PGA.

As an example, Figure 4a shows hazard disaggregation for PGA equal to 0.9g at the site of interest (i.e., L'Aquila). Figure 4b gives $f_{IM_1|IM_2,M,R}$ for $M \in (6, 6.5\text{km})$ and $R_{jb} \in (0\text{km}, 5\text{km})$, which is the scenario dominating the hazard being disaggregated in Figure 4a.

3.4. Reference target fragility

To evaluate the considered conversion cases, the PGA-based (reference) fragility curve was also computed by performing NLDA via MSA; i.e., as in Section 3.2 but with respect to PGA rather than $Sa(0.5s)$. The record selection was analogous to $Sa(0.5s)$ (i.e., 20 GM records fitting the CS given PGA). Figure 5 provides the mean spectra of GM records conditioned at PGA and the MSA results. A smaller number of failure cases was observed in this case (5 vs 14 failure cases at the tenth IM level; see Figure 2). Hence, the analysis was also performed at the two additional IM levels corresponding to $T_R = 10^6$

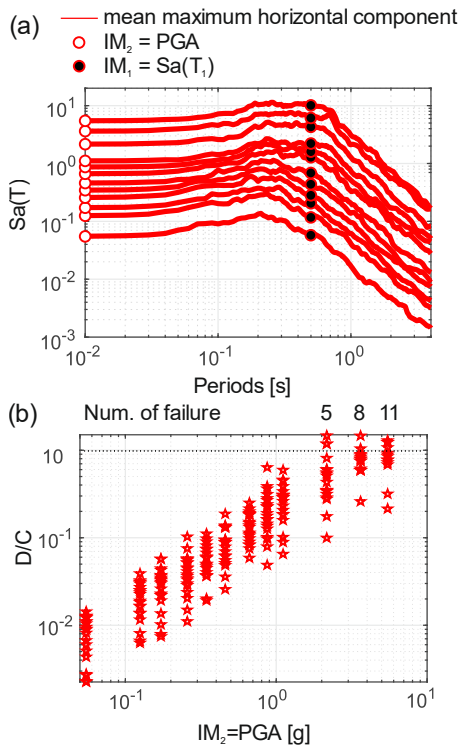

Figure 5: MSA for reference target fragility; (a) mean spectra of GM records; (b)D/C ratios and number of failure cases.

and $T_R = 10^7$ years so as to observe failure cases in at least 50% of the records. The target lognormal fragility was fitted through a maximum likelihood estimation criterion (Baker, 2015).

3.5. Conversion results

The PGA-based fragility curves were derived from the presented fragility and hazard models through the conversion formulas of Eqs. (1)-(3). The results of the three conversion strategies, each involving $\mathbf{IM}_{4v}$, $\mathbf{IM}_{2v}$ and IM_1, are presented in Figure 6, together with the reference fragility curve described in Section 3.4. As seen in the figure, the $\mathbf{IM}_{4v}$ case provided the curve closest to the reference, while all cases provided apparently comparable results, showing the curves located slightly at the left side of the reference case. In fact, the median PGA causing failure $(PGA_{f.50\%})$ and the standard deviation (β), computed as the difference between the 16th and 50th percentiles of each converted curve,

resulted in less than 12% difference with respect to the reference target in all cases (Table 4).

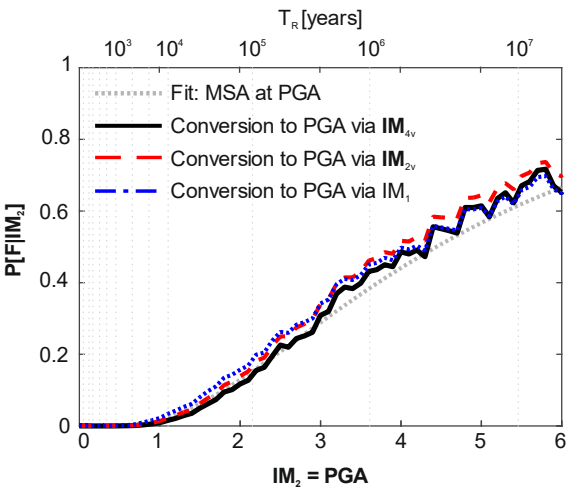

Figure 6: Converted and reference fragility curves.

Table 4: Comparisons of the conversion strategies.

Parameter\IM	***Approach***			
	IM $_{4v}$	**IM** $_{2v}$	IM_1	***Reference***
$PGA_{f.50\%}$ [g]	*4.34*	*3.96*	*4.19*	*4.46*
Difference	*-3%*	*-11%*	*-6%*	*0%*
β	*0.65*	*0.62*	*0.72*	*0.71*
Difference	*-8%*	*-12%*	*-2%*	*0%*

All the converted curves appear to be similar, likely because of the fact that the two GM characteristics considered herein are accounted for through the hazard-consistent record selection via the CS approach, as well as owing to the relative-sufficiency of the original IM_1 with respect to structural response.

4. CONCLUSIONS

The presented study discussed equations for converting IMs of fragility functions with the aid of the state-of-the art methods within PBEE, without any additional structural analyses.

On the premise that structural response given an IM is available from a preliminary analysis, three possible conversion cases with different assumptions on the IMs involved, were discussed. In all cases, the fragility in terms of the target IM was computed based on the total probability theorem.

The considered conversion cases were illustrated through the application study using the ESDoF system of an Italian code-conforming RC building. The PGA fragility curves were obtained from the structural response given $Sa(T)$ and then were compared with a reference fragility directly developed in terms of the target IM.

As far as the case study is concerned, all cases provided the parameters of the converted curves within 12% difference from those of the reference fragility (the four-variables conversion, involving the original and target IMs, magnitude and distance, resulted to be the closest as expected). This is likely owing to the hazard-consistent record selection according to the CS approach and to the explanatory power of the original IM; i.e., $Sa(T)$ for the structural response analysis.

5. ACKNOWLEGEMENTS

The study presented in this article was developed within the activities of the ReLUIS-DPC 2014-2018 research program, funded by *Presidenza del Consiglio dei Ministri – Dipartimento della Protezione Civil* and the Horizon 2020 MSCA-RISE-2015 project No. 691213 entitled *"Experimental Computational Hybrid Assessment of Natural Gas Pipelines Exposed to Seismic Risk" (EXCHANGE-RISK)*.

6. REFERENCES

Ambraseys, N. N., Simpson, K. A., and Bommer, J. J. (1996). "Prediction of horizontal response spectra in Europe." *Earthq. Eng. Struct. Dyn.*, 25(4), 371–400.

Baker, J. W. (2007). "Probabilistic structural response assessment using vector-valued intensity measures." *Earthq. Eng. Struct. Dyn.*, 36(13), 1861–1883.

Baker, J. W. (2015). "Efficient analytical fragility function fitting using dynamic structural analysis." *Earthq. Spectra*, 31(1), 570–599.

Baker, J. W., and Cornell, A. C. (2005). "A vector-valued ground motion intensity measure consisting of spectral acceleration and epsilon."

Earthq. Eng. Struct. Dyn., 34(10), 1193–1217.

Baker, J. W., and Jayaram, N. (2008). "Correlation of spectral acceleration values from NGA ground motion models." *Earthq. Spectra*, 24(1), 299–317.

Baltzopoulos, G., Baraschino, R., Iervolino, I., and Vamvatsikos, D. (2017). "SPO2FRAG: software for seismic fragility assessment based on static pushover." *Bull. Earthq. Eng.*, 15(10), 4399–4425.

Bazzurro, P., and Cornell, A. C. (1999). "Disaggregation of seismic hazard." *Bull. Seismol. Soc. Am.*, 89(2), 501–520.

CEN. (2004). "Eurocode 8: Design Provisions for Earthquake Resistance of Structures, Part 1.1: General rules, seismic actions and rules for buildings, EN1998-1."

Chioccarelli, E., Cito, P., Iervolino, I., and Giorgio, M. (2018). "REASSESS V2.0: software for single- and multi-site probabilistic seismic hazard analysis." *Bull. Earthq. Eng.*, 1–25.

Cornell, A., Asce, M., Jalayer, F., Hamburger, R. O., and Foutch, D. A. (2002). "Probabilistic basis for 2000 SAC federal emergency management agency steel moment frame guidelines." *J. Struct. Eng.*, 128(4), 526–533.

Cornell, A. C., and Krawinkler, H. (2000). *Progress and challenges in seismic performance assessment,* PEER Center News, 3, 1-3, CA, USA.

Elefante, L., Jalayer, F., Iervolino, I., and Manfredi, G. (2010). "Disaggregation-based response weighting scheme for seismic risk assessment of structures." *Soil Dyn. Earthq. Eng.*, 30(12), 1513–1527.

Iervolino, I., Giorgio, M., Galasso, C., and Manfredi, G. (2010). "Conditional hazard maps for secondary intensity measures." *Bull. Seismol. Soc. Am.*, 100(6), 3312–3319.

Iervolino, I., Spillatura, A., and Bazzurro, P. (2018). "Seismic reliability of code-conforming Italian buildings." *J. Earthq. Eng.*, 22(sup2), 5–27.

Jalayer, F., and Cornell, A. C. (2003). *A Technical Framework for Probability-based Demand and Capacity Factor Design (DCFD) Seismic Formats,* PEER Report 2003/08, CA, USA.

Joyner, W., and Boore, D. (1981). "Peak horizontal acceleration and velocity from strong-motion records including records from the 1979 Imperial Valley, California, earthquake." *Bull. Seismol. Soc. Am.*, 71(6), 2011–2038.

Lin, T., Haselton, C. B., and Baker, J. W. (2013). "Conditional spectrum-based ground motion selection. Part I: Hazard consistency for risk-based assessments." *Earthq. Eng. Struct. Dyn.*, 42(12), 1847–1865.

Michel, C., Crowley, H., Hannewald, P., Lestuzzi, P., and Fäh, D. (2018). "Deriving fragility functions from bilinearized capacity curves for earthquake scenario modelling using the conditional spectrum." *Bull. Earthq. Eng.*, 16(10), 4639–4660.

Ohtori, Y., and Hirata, K. (2007). *Conversion Methods of Ground Motion Index for Fragility Curve,* CRIEPI Civil Engineering Research Laboratory Rep.No.N05053, Tokyo, Japan.

Ricci, P., Manfredi, V., Noto, F., Terrenzi, M., Petrone, C., Celano, F., De Risi, M. T., Camata, G., Franchin, P., Magliulo, G., Masi, A., Mollaioli, F., Spacone, E., and Verderame, G. M. (2018). "Modeling and Seismic Response Analysis of Italian Code-Conforming Reinforced Concrete Buildings." *J. Earthq. Eng.*, 22(sup2), 105–139.

Shome, N., and Cornell, A. C. (2000). "Structural seismic demand analysis: consideration of 'collapse.'" *Proc. 8th ACSE Spec. Conf. Probabilistic Mech. Struct. Reliab.*, South Bend, Indiana, USA.

Stucchi, M., Meletti, C., Montaldo, V., Crowley, H., Calvi, G. M., and Boschi, E. (2011). "Seismic hazard assessment (2003-2009) for the Italian building code." *Bull. Seismol. Soc. Am.*, 101(4), 1885–1911.

Suzuki, A., Baltzopoulos, G., Iervolino, I., and RINTC-Workgroup. (2018). "A look at the seismic risk of Italian code-conforming RC buildings." *Proc. 16th Eur. Conf. Earthq. Eng.*, 18–21Thessaloniki, Greece.

Tothong, P., and Luco, N. (2007). "Probabilistic seismic demand analysis using advanced ground motion intensity measures." *Earthq. Eng. Struct. Dyn.*, 36(13), 1837–1860.

Vamvatsikos, D., and Cornell, A. C. (2006). "Direct estimation of the seismic demand and capacity of oscillators with multi-linear static pushovers through IDA." *Earthq. Eng. Struct. Dyn.*, 35(9), 1097–1117.